이학석사 학위논문

담배 연기 추출물로 인해 유발되는 만성폐쇄성폐질환 마우스 모델을 이용한 포도씨 프로안토시아니딘 추출물의 폐기종 억제 기전 규명

Inhibitory Mechanism of Grape Seed Proanthocyanidin Extract against Cigarette Smoke Extract-induced Emphysema using a Mouse Model of Chronic Obstructive Pulmonary Disease

울산대학교대학원
의과학과
최혜원

담배 연기 추출물로 인해 유발되는 만성폐쇄성폐질환 마우스 모델을 이용한 포도씨 프로안토시아니딘 추출물의 폐기종 억제 기전 규명

지도교수 나 승 원

이 논문을 이학석사 학위 논문으로 제출함

2024년 02월

울산대학교 대학원
의 과 학 과
최 혜 원

최혜원의 이학석사학위 논문을 인준함

심사위원 권 병 석 (인)
심사위원 제 갈 양 진 (인)
심사위원 나 승 원 (인)

울 산 대 학 교 대 학 원
2024년 02월

ABSTRACT

Cigarette smoke (CS) increases reactive oxygen species (ROS) production in inflammatory and epithelial cells. ROS enhance autophagy-induced inflammation in alveolar macrophages (AMs), which are the primary source of cytokines and have been implicated in the pathogenesis of chronic obstructive pulmonary disease (COPD). Grape seed proanthocyanidin extract (GSPE) is a flavonoid compound with potent antioxidant and anti-inflammatory effects. However, whether GSPE can inhibit inflammation and emphysema remains unclear. In this study, we aimed to clarify whether GSPE can inhibit emphysema and airway inflammation by ameliorating cigarette smoke extract (CSE)-induced autophagy through the suppression of oxidative stress in macrophages. Results showed that GSPE significantly attenuated CSE-induced emphysema and airway inflammation in mouse lungs. Moreover, GSPE ameliorated lung inflammation by reducing the numbers of total cells, macrophages, and neutrophils and decreasing the levels of tumor necrosis factor-α, interleukin (IL)-1β, and IL-6 in the bronchioloalveolar lavage fluid. ROS levels increased after CSE treatment but clearly decreased with *in vitro* GSPE treatment. GSPE decreased transcription factor EB (TFEB) oxidation by reducing ROS production, consequently inhibiting TFEB nuclear translocation. Furthermore, GSPE suppressed ROS-induced autophagy in RAW 264.7 cells, bone marrow-derived macrophages, and AMs. Consequently, it diminished CSE-induced lung inflammation by inhibiting the NLR family pyrin domain containing 3 (NLRP3) inflammasome. These results suggest that GSPE ameliorates CSE-induced inflammation and emphysema by regulating autophagy-induced NLRP3 inflammasome through the ROS/TFEB signaling pathway in a COPD mouse model.

Keywords: Chronic Obstructive Pulmonary Disease, Cigarette smoke extract, Grape seed proanthocyanidin extract, Inflammation, Emphysema, Oxidative stress, Autophagy

CONTENTS

LIST Of FIGURES

Introduction

Chronic obstructive pulmonary disease (COPD) is a progressive, irreversible inflammatory disease of the lungs that involves loss of alveolar surface area (emphysema) and airway inflammation (chronic bronchitis), which limit airflow [1, 2]. COPD is a major cause of morbidity and mortality worldwide, and its incidence increases annually. The etiology of COPD potentially involves imbalances in inflammation, redox homeostasis, and protease/antiprotease equilibria, which are related to smoke exposure [3, 4]. However, the mechanisms underlying COPD pathogenesis remain incompletely understood.

Cigarette smoke (CS) exposure is a major etiologic factor for COPD [5]. CS contains more than 4,700 chemicals, including several highly reactive oxygen species (ROS). Thus, CS can enhance ROS production in inflammatory and epithelial cells [4, 6, 7]. Excessive ROS production in the respiratory tract, lungs, and blood of patients with COPD leads to oxidative modifications in proteins, lipids, and DNA [8]. In addition, CS-induced oxidative stress results in chronic inflammation and recruitment of inflammatory cells, primarily alveolar macrophages (AMs) and neutrophils, to the airways. Lung AMs, the primary source of cytokines in response to inflammatory stimuli [9], participate in lung injury pathogenesis by initiating inflammatory responses and facilitating neutrophil infiltration and tissue damage in the lungs [10]. In macrophages, CS enhances autophagy activation [11, 12]. Moreover, AMs have been implicated in the pathogenesis of COPD and CS-related lung diseases, such as acute lung injury [13, 14]. However, their roles in CS-related lung disease remain unclear.

Autophagy is a regulated process for the turnover of cytoplasmic proteins and organelles through lysosome-dependent mechanisms. During this process, double-membraned autophagosomes sequester organelles, protein aggregates, or pathogens and fuse with a lysosome to form an autolysosome for the degradation or recycling of cytoplasmic components. Autophagy is a critical and conserved cellular survival mechanism to maintain cellular homeostasis [15, 16]. This process can be induced under pathological conditions to protect cells from injurious stimuli or, alternatively, induce irreversible tissue injury [17-20]. Chen et al. reported that cigarette smoke extract (CSE)-induced oxidative stress increases LC3-II accumulation, which is enhanced by bafilomcyin A1 and lysosomal protease inhibitors, indicating that CSE-induced oxidative stress promotes autophagy [17, 19]. Additionally,

autophagy is important in regulating innate immunity and inflammation [18]. Specifically, it has been suggested to regulate the release of proinflammatory cytokines. Zhang et al. reported that autophagy in macrophages regulates early lung inflammation during mechanical ventilation through NLR family pyrin domain containing 3 (NLRP3) inflammasome signaling [20]. Furthermore, during lipopolysaccharide-induced lung inflammation, autophagy deficiency in macrophages decreases lung and bronchoalveolar immune cell infiltration and cytokine levels in the air space [21]. However, the exact functions of autophagy in pulmonary macrophages in CSE-induced COPD pathogenesis remain unclear.

The NLRP3 inflammasome is a cytosolic multi-protein complex that is primarily expressed in monocytes and macrophages [22, 23]. It is a component of the innate immune response that can enhance the secretion of interleukin (IL)-1β and IL-18 through caspase-1 activation, resulting in resistance to the damage caused by some pathogens. However, overactivation of the NLRP3 inflammasome can lead to various inflammatory lung diseases, including COPD. Numerous studies have utilized various agents, including the antioxidant drug cysteamine [24], Vitamin E [25], 4-phenyl butyric acid [26], and the mitophagy inhibitor Mdivi1 [27], to ameliorate the aberrant autophagy induced by smoke exposure in mouse models. However, research on this topic is currently limited; thus, additional studies are needed to discover novel antioxidant drugs.

Grape seed proanthocyanidin extract (GSPE) is a flavonoid compound with various pharmacological properties, such as antioxidant [28], anticarcinogenic [29], antiallergic [30], anti-inflammatory [31], antihypertensive [32], and antiviral [33]. Additionally, GSPE ameliorates amiodarone-induced lung toxicity [34] and bleomycin-induced pulmonary fibrosis [35]. Considering that autophagy can be induced with CSE-induced oxidative stress and contributes to lung inflammation and emphysema, we hypothesized that GSPE as an antioxidant can reduce CSE-induced oxidative stress and autophagy, consequently suppressing inflammation and emphysema. We further aimed to investigate whether GSPE alleviates autophagy-induced NLRP3 inflammasome induction by inhibiting the ROS/transcription factor EB (TFEB), resulting in the amelioration of CSE-induced lung inflammation and emphysema in a COPD mouse model.

Materials and methods

1. Animal experiments

Specific pathogen-free (SPF) 6-week-old female BALB/c mice weighing between 18 and 20 g were purchased from Koatech Co. (Pyongtaek, Korea). The mice were housed in an SPF animal facility and used after a week of acclimatization. This study was approved by the Institutional Review Board (IRB) of Ulsan University Hospital (UUH; IRB No. NON2022-002) and the Institutional Animal Care and Use Committee (IACUC; No. A-221012-01). After a week of acclimation, the mice were randomly divided into six groups (n = 8 per group): (1) phosphate-buffered saline (PBS): mice treated with PBS; (2) CSE+PBS: mice injected with CSE and PBS; (3) PBS+GSPE: mice injected with PBS and 100 mg/kg GSPE; (4–6) CSE+GSPE (25, 50, or 100 mg/kg): mice intraperitoneally injected with 25, 50, or 100 mg/kg GSPE 30 min before CSE injection. The mice were intraperitoneally injected with 0.2 mL of CSE on days 1, 8, 15, and 23 and then sacrificed on day 28.

2. Reagents and antibodies

Enzyme-linked immunosorbent assay (ELISA) kits for tumor necrosis factor (TNF)-α, IL-1β, and IL-6 were purchased from BD Biosciences (Cambridge, MA, USA). GSPE was provided by Hanlim Pharmaceuticals (Entelon®, Seoul, Korea). CM-H_2DCFDA was purchased from Invitrogen (C6827, Carlsbad, CA, USA). Hoechst 33342 (H3570), 3-methyladenine (3-MA, M9281), and N-acetyl-L-cysteine (NAC; A9165) were obtained from Sigma Chemical (St. Louis, MO, USA). N-(Biotinoyl)-N′-(iodoacetyl) ethylenediamine (BIAM; AS-60644) was obtained from AnaSpec (Fremont, CA, USA). Cyto-ID autophagy detection kit 2.0 (ENZ-KIT175-0050) and the CellTiter 96TM aQueous One Solution Cell Proliferation Assay (MTS; G3580) were purchased from Promega (Madison, WI, USA). SureBeads™ Protein G Magnetic beads were purchased from Bio-Rad (#161-4023). The following primary antibodies were used for analysis in this study: antibodies against TFEB (A303-673A) from Bethyl Laboratories Inc. (Montgomery, TX, USA) and LC3B (#2775) from Cell Signaling Technology (Danvers, MA, USA). Lamin B1 (#13435) and β-actin (A5441) used as internal controls were obtained from Invitrogen (San Diego, CA, USA). Horseradish peroxidase (HRP)-labeled secondary anti-mouse (#7076) and anti-rabbit (#7074) antibodies were purchased from Cell Signaling Technology. APC rat and anti-F4/80 antibody (1:100,

566787; BD Biosciences, USA) was purchased from BD Biosciences. Anti-rabbit IgG Fab2 Alexa Fluor® 488 molecular probes (1:2000, A-11070) as a secondary antibody were obtained from Invitrogen.

3. Preparation of CSE

CSE was prepared as previously described [8]. Briefly, three cigarettes (3R4F reference cigarette from The Tobacco and Health Research Institute, University of Kentucky, USA) were burned, and the smoke was passed through 10 mL of PBS at a constant airflow rate using a peristaltic pump (VWR International). Then, the CSE-PBS solution adjusted to pH 7.2–7.4 was filtered through a 0.22 μm filter, which was considered 100% CSE and used within 1 h of CSE preparation. For *in vitro* studies, a cigarette was burned, and the smoke was collected into 10 mL of RPMI-1640 using a peristaltic pump (VWR International).

4. Morphological assessment of lung tissues

The lung tissues were fixed in 3% paraformaldehyde and dehydrated with graded ethanol solutions. After embedding in paraffin, 4-μm-thick sections were prepared and stained with hematoxylin and eosin (H&E). The mean linear intercept (MLI) (μm) and destructive index (DI) (%) were measured to quantify emphysema as described previously [36, 37]. Briefly, the MLI was measured by dividing the length of a line drawn across the lung section by the total number of intercepts counted within this line. The DI was calculated by dividing the defined destructive alveoli by the total number of alveoli.

5. Bronchoalveolar lavage fluid preparation and total cell and leukocyte counts

On day 28, bronchoalveolar lavage fluid (BALF) was collected by instilling an initial 1 mL of sterile PBS, followed by two washes with 500 μL of PBS. The fluid was centrifuged at 1500 rpm for 5 min, and the supernatant of the BALF was used to determine cytokines. The cell pellet was resuspended in 1 mL of PBS, and the total cell count in the BALF was measured with a hemocytometer. The resuspended cells were diluted to a final concentration of 2.5×10^5 cells/mL, and 200 μL of cells was cytospun onto slides at 800 rpm for 5 min with a Thermo-Shandon Cytospin 4 cytofuge (Thermo Fisher Scientific, Waltham, MA, USA). The slides were stained with Wright−Giemsa stain, and 300 leukocytes were counted on each slide. The numbers of neutrophils and macrophages were counted.

6. Cell culture

Mouse macrophage RAW 264.7 cells (KCLB, Seoul, Korea) were grown in RPMI 1640 medium (Welgene, Daegu, Korea) supplemented with 10% FBS and 1% penicillin–streptomycin solution at 37 °C in a humidified atmosphere with 5% CO_2. RAW 264.7 cells were pretreated with GSPE (3 μg/mL) for 4 h and then stimulated with 3% CSE for an additional 24 h.

7. Isolation and culture of mouse bone marrow-derived macrophages

Bone marrow-derived macrophages (BMMs) were obtained as described previously [38]. Briefly, the femora and tibiae were aseptically removed from the mice. The marrow cavity was washed with Dulbecco's modified Eagle's medium from one end of the bone using a sterile 21-gauge needle after dissecting the bone ends. The resulting bone marrow suspension was washed twice and incubated on plates with mouse stem cell factor (30 ng/mL) for 16 h. Floating cells were harvested; after 2 days of incubation, large populations of monocyte/macrophage-like cells adhered to the culture plates. Floating cells were discarded by washing dishes with PBS, and the adherent cells (BMMs) were collected and seeded on plates.

8. Isolation of AMs from lungs

AMs were isolated from mouse lungs as described previously [7]. Briefly, BALF was collected by washing the lung with an initial 1 mL of sterile PBS, followed by two 500 μL PBS washes. The fluid was centrifuged at 1500 rpm for 5 min, and a differential cell count was performed after washing the lavage cells. Lavage fluid from mice contained 98% AMs, and the AMs were 96% viable, as determined by a trypan blue exclusion assay.

9. Cell viability assay

RAW 264.7 cells were cultured in a 96-well plate at 3×10^4 cells per well and grown to 80% confluency. The cells were then treated with CSE at the indicated concentrations (0%, 3%, 5%, 10%, 15%, and 20 %). An MTS assay was performed using CellTiter 96 aQueous One Solution Cell Proliferation Assay (Promega) in accordance with the manufacturer's instructions, and the optical densities of the samples were determined using a spectrophotometer at 490 nm.

10. Intracellular ROS measurement

Intracellular ROS was detected using the fluorescent probe 2′,7′-dichlorofluorescein diacetate (CM-H_2DCFDA). RAW 264.7 cells were pretreated with GSPE (3 μg/mL) for 4 h following 3% CSE stimulation for 15 h. Then, the cells were rinsed briefly in PBS and incubated with culture medium containing 5 μM CM-H_2DCFDA at 37 °C for 30 min in the dark. Fluorescence was detected by flow cytometry (FACSCanto II), and the data were analyzed using FlowJo V10 software (Tree Star Inc., San Carlos, CA). RAW 264.7 cells were grown on glass cover slips in 24-well plates, and then ROS levels were measured using confocal microscopy. The cells were pretreated with GSPE (3 μg/mL) for 4 h and then stimulated with 3% CSE for 15 h. After staining with 10 μM CM-H_2DCFDA for 15 min, the cover slips were removed from the wells of the plate and placed on a slide for analysis. Fluorescence images were analyzed using an Olympus FV1200 confocal microscope (Olympus, Tokyo, Japan).

11. Immunofluorescence

AMs were seeded onto sterile glass coverslips in a 24-well flat-bottomed microplate at 5 × 10^4 cells/well and then incubated in RPMI-1640 medium supplemented with 10% FBS and 1% penicillin–streptomycin solution at 37 °C in a humidified atmosphere with 5% CO_2. The cells were pretreated with GSPE (3 μg/mL) for 4 h and then stimulated with 3% CSE for an additional 24 h. The culture medium was removed from the coverslips, and all the cultured cells were fixed with 4% ice-cold formaldehyde for 10 min and then permeabilized with 0.2% Triton X-100 (Sigma-Aldrich) in PBS. The samples were pre-blocked with 1% bovine serum albumin for 30 min at room temperature to reduce nonspecific staining. The cells were probed with an anti-LC3BII antibody (1:100) and APC rat and anti-mouse F4/80 antibody (1:100) at 4 °C overnight and subsequently detected with anti-rabbit IgG Fab2 Alexa Fluor® 488 molecular probes (1:2000). The immunofluorescence images were obtained using an Olympus FV3000 confocal microscope (Olympus).

12. RNA isolation and quantitative polymerase chain reaction (qPCR)

Total RNA was extracted from cells using QIAzol reagent and reverse-transcribed with random primers and M-MLV reverse transcriptase (Promega, Madison, USA). qPCR was carried out using SYBR Green Taq polymerase (Qiagen, Hilden, Germany) on a StepOnePlus Real-Time PCR System (Applied Biosystems, Foster City, CA, USA). The housekeeping gene *18S rRNA* (*RPS*) was amplified in parallel with the genes of interest. The relative amount of

transcript was calculated using the $2^{-\Delta\Delta CT}$ method. The following primers were used: 5′-TGT GGA ACA TGG AGG GAA GAG-3′ and 5′-TGT GCC TGT GCT GGA ACT TTC-3′ (*p62/SQSTM1*); 5′-TGA AAT CAA TGC TGC CTG GG-3′ and 5′-CCA GAA CAG TAT AAC GGC AAC TCC-3′ (*BECLIN 1*); 5′-ATG GGA GTT GGC GAA GGC AAG T-3′ and 5′-CAG CCA AGG AAC TCC ATG TGT C-3′ (*ATG 4b*); 5′-GAG CAG GAC TAT GAA CGG CTA G-3′ and 5′-GTC CAG GTT CTG GAT GTG ATG C-3′ (*ATG 9b*); 5′-ATC AGA GAG TTG ACC GCA GTT G-3′ and 5′-AAT GAA CCG AAG CAC ACC ATA G-3′ (*RPS*).

13. Nuclear and cytosolic fractionation

To detect the localization of TFEB, we fractionated RAW 264.7 cells by using a nuclear and cytosol fractionation kit in accordance with the manufacturer's protocol. Proteins were separated by sodium dodecyl-sulfate polyacrylamide gel electrophoresis (SDS-PAGE) and transferred onto nitrocellulose membranes. The membranes were blocked with 5% skim milk in Tris-buffered saline containing 0.05% Tween 20 (1X TBS-T) for 1 h at room temperature and then incubated overnight at 4 °C with primary antibodies against TFEB, Lamin B1, and β-actin. After being washed with 1X TBS-T, the membranes were incubated with HRP-conjugated secondary antibodies for 1 h at room temperature and developed using the ECL detection system (GE Healthcare, Waukesha, WI).

14. Western blot analysis

Total proteins from RAW 264.7 cells and BMMs were extracted on ice with lysis buffer (50 mM Tris-HCl, pH 8.0, 150 mM NaCl, 1 mM EDTA, 0.5% Nonidet P-40, and 0.01% protease inhibitor mixture). After centrifugation for 15 min at 16,000 × g, the supernatants were recovered. The protein concentration was determined using the BCA protein assay kit (Pierce Biotechnology, Rockford, IL, USA). Typically, 20 μg of protein per lane was loaded on SDS-PAGE gels and transferred onto nitrocellulose membranes. The membranes were blocked for 1 h with 5% skim milk in PBS containing 0.05% Tween 20 (PBS-T) and then incubated overnight at 4 °C with primary antibodies against LC3BII, TFEB, Lamin B1, and β-actin. After being washed with PBS-T, the membranes were incubated for 1 h with HRP-conjugated secondary antibodies and developed using the ECL detection system.

15. Immunoprecipitation

Total lysate of RAW 264.7 cells was subjected to immunoprecipitation (IP) using an anti-

NLRP3 antibody with SureBeads magnetic beads (Novex, ThermoFisher Scientific, Waltham, MA, USA). The anti-NLRP3 antibody (1 μg) was incubated with total protein lysate (1 mg) overnight at 4 °C and then incubated with magnetic beads for 3 h at 4 °C. After being washed with PBS-T, the tube was placed on the magnet. The supernatant was analyzed by immunoblotting for ASC, cleaved caspase-1, and NLRP3 antibodies.

16. Transfection of siRNA

RAW 246.7 cells were seeded in 24-well plates at 2×10^5 cells/well and grown for 24 h. The cells were transfected with small interfering RNA (siRNA) against ATG5, TFEB or with scrambled siRNA (scRNA) using Lipofectamine 3000 and then incubated in the presence or absence of 3% CSE for 24 h.

17. Measurement of cytokines

Cytokines were analyzed in the BALF recovered from mice or in the cell culture supernatants. The concentrations of TNF-α, IL-1β, and IL-6 were measured using ELISA kits in accordance with the manufacturer's instructions (R&D Systems).

18. Detection of acidic vesicular organelles

To characterize autophagy, we quantified acidic vesicular organelles (AVOs; i.e., autolysosomes) by using flow cytometry after staining with acridine orange (AO) as described previously [39]. The cells were stained with AO (1 μg/mL) for 20 min, washed twice, and analyzed by using flow cytometry (FACSCanto II).

19. Detection of oxidized TFEB via carboxymethylation

RAW 264.7 cells were preincubated with GSPE (3 μg/mL) for 4 h and then cultured in a medium with 3% CSE for an additional 15 h. Then, the medium was removed, and the cells were snap-frozen in liquid nitrogen. Radioimmunoprecipitation (RIPA) buffer containing 100 M BIAM (Molecular Probes, Invitrogen, Carlsbad, CA) was rendered free of oxygen by bubbling with nitrogen gas at a low flow rate for 20 min. The frozen cells were lysed in 700 μL of RIPA buffer with protease inhibitor and then incubated for 15 min at room temperature. Lysates were clarified by centrifugation and immunoprecipitated with 1 μg of TFEB-specific antibody (Bethyl Laboratories). Immunocomplexes labeled with BIAM were detected with HRP-conjugated streptavidin and developed with an enhanced chemiluminescence kit.

20. Electrophoretic mobility shift assay (EMSA)

Nuclear protein extracts were obtained from RAW 264.7 macrophages stimulated with GSPE (3 μg/mL) or NAC (5 mM) in accordance with the manufacturer's manual (LightShift Chemiluminescent EMSA kit). Susbequently, 3 μg of nuclear extract was added to 20 fmol biotin-labeled oligonucleotides (TFEB, 5′-GTA GGC CAC GTG ACC GGG-3′; NF-Y, 5′ -AGA CCG TAC GTG ATT GGT TAA TCT CTT-3′) and then incubated with 1X binding buffer, 50 ng/mL poly(dI-dC), 0.05% Nonidet P-40, 5 mM $MgCl_2$, 10 mM EDTA, and 2.5% glycerol for 20 min at room temperature. The reactions were analyzed by electrophoresis on 3% polyacrylamide gels in 0.5X TBE buffer at 40 V for 80 min and then transferred onto positively charged nylon membranes in 0.5X TBE at 40 V for 60 min. The transferred DNA was crosslinked to the membranes at 10 mJ/cm^2 and detected using HRP-conjugated streptavidin.

21. Autophagosome quantification

RAW 264.7 cells were grown on glass cover slips in 24-well plates, and autophagy was measured using the Cyto-ID autophagy detection kit (ENZ-51031-0050). RAW 264.7 cells were pretreated with GSPE (3 μg/mL) for 4 h, stimulated with 3% CSE for 15 h, and then stained with Cyto-ID Green dye and Hoechst 33342 at 37 °C for 30 min in accordance with the manufacturer's instructions. The coverslips were removed from the wells of the plate and placed on a slide for confocal microscopic analysis. Fluorescence images were analyzed using an Olympus FV1200 confocal microscope.

22. Statistical analyses

All values are expressed as means ± standard error of the mean (SEM). Each series of experiments was repeated at least three times. Considering that the sample means were normally distributed, we used one-way analysis of variance (ANOVA) for comparisons of more than two groups, followed by Bonferroni post-tests, and the t-test for two-group comparisons. Statistical analyses were performed using GraphPad Prism 5 (GraphPad Prism Software Inc., CA, USA) and SPSS 24.0 (SPSS, Inc., IL, USA). A p value < 0.05 was considered statistically significant.

Results

1. GSPE ameliorates CSE-induced lung inflammation and emphysema

GSPE exerts potent antioxidant and anti-inflammatory effects on inflammatory diseases, including lung disease [31, 35, 40]. Therefore, we hypothesized that GSPE can ameliorate the development of CSE-induced COPD by attenuating oxidative stress and inflammation. To investigate the effect of GSPE on the molecular pathogenesis of COPD, we first established a CSE-induced COPD mouse model. For histopathological analysis, lung sections were stained with H&E. Intraperitoneal injection of CSE in the mice led to inflammation and emphysematous lung destruction within 28 days. H&E staining revealed peribronchial interstitial infiltration of inflammatory cells as well as alveolar edema. Emphysema was greater in the CSE-treated group than in the PBS-treated group (Fig. 1A). Airspace enlargement and destruction of alveolar walls were evaluated based on the MLI and DI, respectively, and both significantly increased in the mice exposed to CSE (Fig. 1B), indicating that CSE contributed to airspace enlargement and the destruction of alveolar walls, which is a structural feature of emphysema [41]. By contrast, the GSPE+CSE group showed significant reductions in these parameters compared with those observed in the CSE-only group. The significantly increased alveolar edema in the lung lesions of mice exposed to CSE was ameliorated by GSPE (Fig. 1A, B), indicating the inhibitory effect of GSPE on CSE-mediated COPD in mice.

Furthermore, we determined whether GSPE can ameliorate CSE-induced lung inflammation. Pulmonary macrophages play prominent pathologic roles in humans with COPD [42]. Consistent with these findings, the numbers of macrophages increased in the lungs of CSE-exposed mice (Fig. 1D). However, as shown in Fig. 1D, the total cell count, neutrophils, and macrophages in the BALF were significantly lower in the GSPE+CSE group than in the CSE-only group. The GSPE+CSE group also showed significantly lower lung inflammation scores and TNF-α, IL-1β, and IL-6 levels than the CSE-only group (Fig. 1C, E). These results indicated that GSPE ameliorated the CSE-induced lung inflammation during COPD progression.

2. GSPE attenuates CSE-induced autophagy

CSE-induced oxidative stress can induce autophagy, which contributes to lung inflammation and lung injury. Thus, we examined whether the antioxidant GSPE can reduce autophagy by decreasing CSE-induced oxidative stress. We assessed the cytotoxic effect of CSE on murine macrophage RAW 264.7 cells. As shown in Fig. 2A, cellular toxicity increased significantly after 3% CSE treatment for 24 h. Considering that the cell viability decreased to less than 40% after exposure to CSE at concentrations greater than 5%, we used 3% CSE. To investigate the effects of GSPE pretreatment on CSE-induced autophagy, we first measured the lipidated form of LC3B (LC3BII), a marker of autophagic flux in RAW 264.7 mouse macrophages and BMMs, which are primary macrophages generated from bone marrow cells. As expected, treatment with CSE substantially enhanced LC3BII accumulation in a dose-dependent manner, whereas cotreatment with GSPE (3 μg/mL) significantly inhibited the CSE-induced LC3BII accumulation (Fig. 2B, C). In addition, CSE-upregulated LC3BII formation was significantly decreased by the autophagy inhibitor 3-MA. The hallmark of autophagy is the formation of autophagosomes and autolysosomes, which are formed by the fusion of an autophagosome with a lysosome. To evaluate whether CSE facilitates the formation of AVOs and GSPE reverses this process, we performed flow cytometry using AO fluorescent dye. The cells were stained with AO, a weak fluorescent base that accumulates in acidic spaces and fluoresces bright red. In AO-stained cells, the cytoplasm and nucleolus appear bright green and dim red, respectively, whereas AVOs appear bright red. Thus, the intensity of the red fluorescence is proportional to the degree of acidity and the total volume of AVOs. In the present study, LC3BII accumulation increased after exposure to 2%, 3%, and 4% CSE. Consistent with this result, AVO formation was more significant at 3% than at 2% CSE. Starvation was also tested as a positive control for autophagy induction. Pretreatment with GSPE decreased the CSE-enhanced formation of AVOs and the percentage of cells with AVOs from 41% to 22% (Fig. 2D). A similar pattern was observed in the 3-MA treated group. AVO staining results showed that CSE clearly increased AVO formation, which was inhibited when the cells were cotreated with GSPE, confirming that GSPE can reduce CSE-induced autophagy. Additionally, we used Cyto-ID® Green dye to detect the autophagic vacuoles formed during autophagy. Consistent with Fig. 2B and D, Fig. 2E shows that treatment with CSE induced significant autophagic flux in the cells in comparison with the vehicle, whereas pretreatment with GSPE markedly decreased the CSE-induced increase in autophagic flux.

Moreover, we isolated AMs from mouse BALF and then performed double immunostaining of F4/80 (red) and LC3Bll (green) by using immunocytochemical staining to identify the role of GSPE in the CSE-induced autophagy of AMs. The autophagy activation of AMs was greater in the CSE group than in the vehicle group (Fig. 2F). However, pretreatment with GSPE significantly decreased the CSE-induced LC3BII expression in macrophages. These results suggested that GSPE can apparently reduce CSE-induced autophagy in mouse lung macrophages.

3. GSPE inhibits CSE-induced oxidative stress, leading to reduced autophagy

We sought to elucidate which signal mediates CSE-induced autophagy. CS enhances ROS production in inflammatory cells, such as AMs [43, 44], and elevated ROS formation promotes autophagy [45, 46]. Therefore, we hypothesized that treatment with CSE increases ROS production to enhance macrophage autophagy and that cotreatment with GSPE abolishes the CSE-induced oxidative stress and thus inhibits autophagy. To assess whether GSPE reduces CSE-induced autophagy by inhibiting oxidative stress, we measured intracellular ROS levels in CSE-treated cells by using DCF-DA, which is oxidized by ROS to fluorescence DCF. RAW 264.7 cells and BMMs were pretreated with GSPE (3 μg/mL) for 4 h, exposed to 3% CSE for another 15 h, and then stained with DCF-DA. Subsequently, intracellular ROS levels were measured using confocal microscopy and flow cytometry. As shown in Fig. 3A and B, the RAW 264.7 cells pretreated with GSPE exhibited significantly lower intracellular ROS production than those treated with CSE alone. Similarly, pretreatment of BMMs with GSPE decreased the CSE-induced increase in ROS production (Fig. 3C). These results suggested that GSPE exerted efficient antioxidant effects on CSE-induced oxidative stress in macrophages. Additionally, GSPE pretreatment significantly reduced the CSE-induced increase in LC3BII levels (Fig. 3D). The same pattern was observed with NAC, a ROS scavenger. Removal of ROS by NAC decreased the enhancing effect of CSE on autophagy activation (Fig. 3E). These results indicated that ROS mediated the CSE-induced autophagy, but GSPE pretreatment ameliorated ROS production and thus decreased the CSE-induced autophagy. Moreover, pretreatment with GSPE significantly decreased the CSE-induced increase in intracellular ROS levels. These results suggested that GSPE exhibited antioxidant effects on CSE-induced oxidative stress and ameliorated oxidative stress-mediated autophagy.

4. GSPE reduces CSE-induced TFEB oxidation, resulting in decreased TFEB nuclear translocation

We investigated which molecule was the target for ROS when exerting an effect on autophagy. ROS directly oxidize TFEB, which promotes nuclear localization [47] and the expression of genes associated with autophagy and lysosomes. Therefore, we assessed whether CSE treatment can increase the levels of oxidized TFEB and whether GSPE pretreatment can reduce this CSE-induced increase. As shown in Fig. 4A, CSE treatment decreased the level of reduced TFEB, whereas GSPE pretreatment restored the reduced TFEB in the presence of CSE. Next, we determined whether CSE treatment enhances TFEB nuclear translocation in macrophages and whether ROS affect this process. CSE treatment decreased the nuclear localization of TFEB, but GSPE pretreatment attenuated the effect of CSE (Fig. 4B). The same pattern was observed with NAC. Removal of ROS by NAC significantly diminished the enhancing effect of CSE on the nuclear translocation of TFEB. Collectively, CSE enhanced the oxidized TFEB and thereby facilitated its activity to increase autophagy, leading to inflammation and further lung injury. However, the increased levels of oxidized TFEB after CSE administration were reversed by GSPE pretreatment. These results showed that ROS removal by GSPE or NAC significantly diminished the enhancing effect of CSE on autophagy activation by preventing CSE-induced TFEB nuclear translocation. The increased TFEB transcriptional activity caused by CSE was confirmed by its induced levels of DNA binding activity and the expression of TFEB target gene. The transcriptional activity of TFEB was assessed using EMSA. Compared with the vehicle, CSE alone enhanced the DNA binding activity of TFEB, whereas GSPE reversed this effect. ROS removal by NAC also reduced the inducing effect of CSE (Fig. 4C). Competition assays using excess of unlabeled probes were performed to determine the specificity of DNA–protein complex formation. NF-Y DNA binding activity was measured as a loading control. Consistent with previously reported results [48, 49], the results of the present study showed that TFEB regulated the expression of genes associated with autophagy (*ATG5*, *BECN1*, and *SQSTM1*). Silencing of TFEB attenuated the expression of *SQSTM1*, *BECN1*, *ATG4b*, and *ATG9b* in the presence of CSE (Fig. 4D). Then, we investigated the effects of TFEB on CSE-induced autophagy. Silencing of TFEB attenuated the increasing effects of CSE on AVO formation (Fig. 4E). These results suggested that CSE enhanced TFEB transcriptional activity, mediating oxidative stress-induced autophagy. However, GSPE restored CSE-induced autophagy by decreasing TFEB transcriptional activity.

5. GSPE attenuates autophagy-induced lung inflammation by inhibiting NLRP3 inflammasome

Autophagy regulates the release of proinflammatory cytokines, including IL-1β. The activation of the NLRP3 inflammasome in AM is involved in COPD pathogenesis [50, 51]. In particular, CS promotes activation of the NLRP3 inflammasome, increasing the release of proinflammatory cytokines, such as IL-1β and IL-18, in human alveolar epithelial cells [52]. Therefore, we hypothesized that inhibition of autophagy through GSPE treatment would diminish CSE-induced lung inflammation by inhibiting the NLRP3 inflammasome. RAW 264.7 cells were pretreated with GSPE (3 μg/mL) for 4 h and then stimulated with 3% CSE for an additional 24 h. The expression levels of NLRP3 inflammasome assembly markers, including NLRP3, ASC, and caspase-1, were determined through western blot. As shown in Fig. 5A, the levels of ASC and caspase-1 proteins clearly increased in the macrophages exposed to 3% CSE. However, GSPE significantly abolished the CSE-induced increase in the expression levels of these NLRP3 inflammasome assembly markers. We confirmed that autophagy mediated the effect of CSE on NLRP3 inflammasome activation. Loss of autophagy by pharmacological inhibition or siRNA silencing of *ATG5* dramatically diminished the enhancing effect of CSE on NLRP3 inflammasome activation. Consistent with this result, the autophagy inhibitor 3-MA also significantly decreased CSE-upregulated NLRP3 inflammasome (Fig. 5B). Moreover, *ATG5* knockdown using siATG5 reduced the expression of the NLRP3 inflammasome in the presence CSE (Fig. 5C). These results indicated that GSPE can regulate autophagy-induced NLRP3 inflammasome activation, which was responsible for the CSE-induced lung inflammation during COPD progression (Fig. 6).

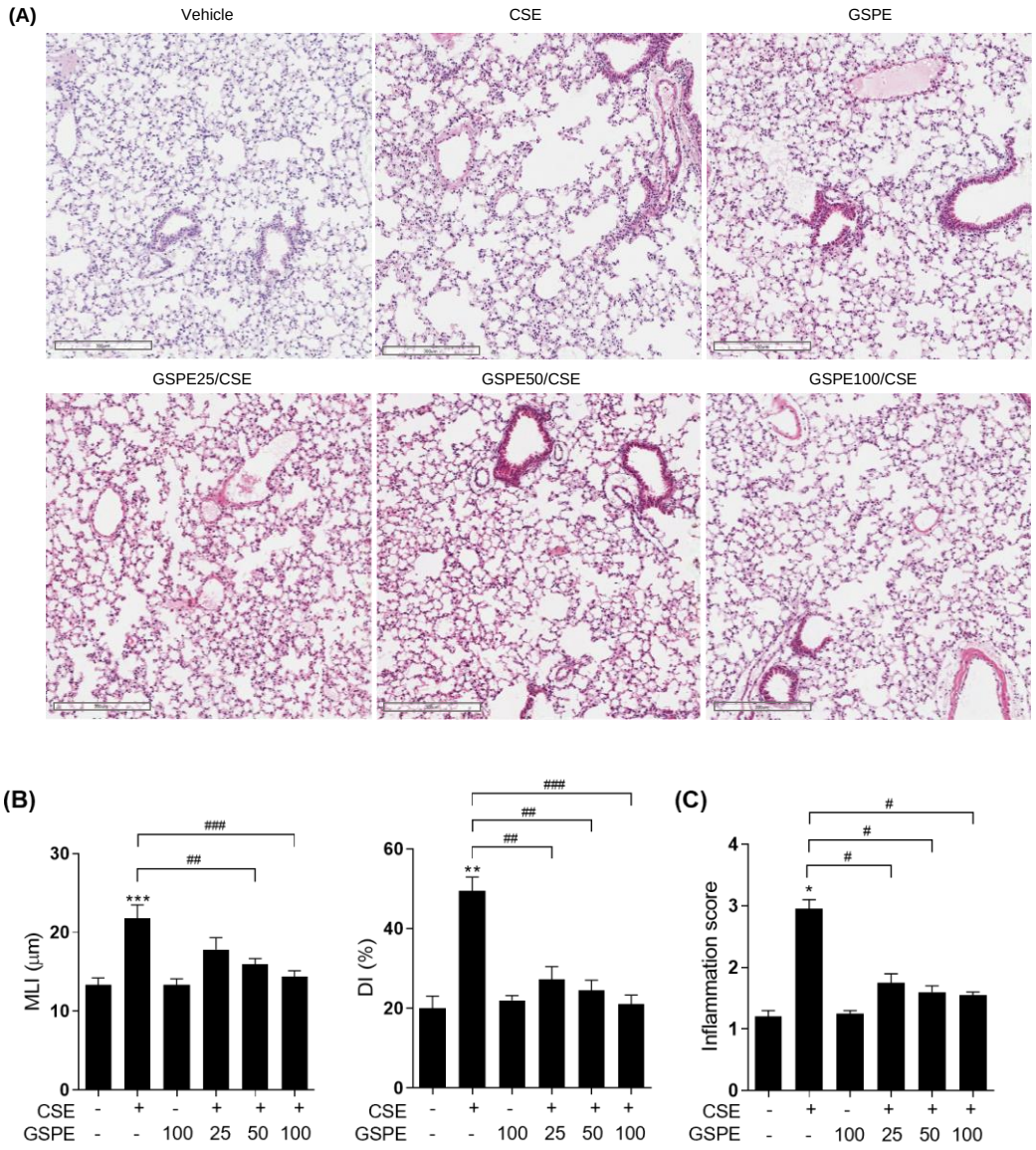

Fig. 1. (continued)

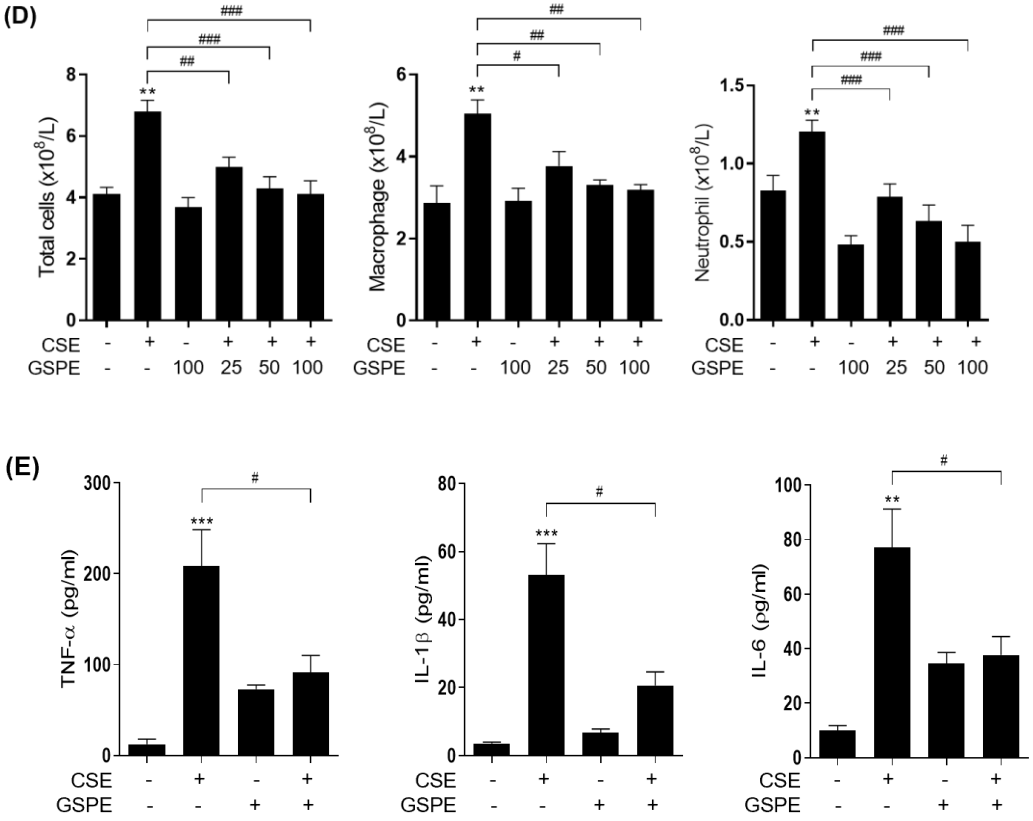

Fig. 1. GSPE ameliorates CSE-induced lung inflammation and emphysema in mice.

BALB/c mice were treated with 25, 50, or 100 mg/kg GSPE 30 min before CSE injection and then intraperitoneally injected with 0.2 mL of CSE on days 1, 8, 15, and 23. Panel (A) shows lung sections stained with H&E after 28 days. Original magnification, 80×. Scale bars, 300 μm. (B) Relative to the mice from the CSE + PBS group, the mice from the CSE+GSPE group showed fewer morphometric changes in the mean linear intercept (MLI) (μm) and destructive index (DI) (%); (C) a lower inflammation score; (D) lower numbers of total cells, neutrophils, and macrophages in the BALF; and (E) lower levels of TNF-α, IL-1β, and IL-6 in the BALF. Data are representative of three independent experiments. *$p < 0.05$, **$p < 0.01$, ***$p < 0.001$ in comparison with the PBS group. #$p < 0.05$, ##$p < 0.01$, ###$p < 0.001$ in comparison with the CSE+PBS group.

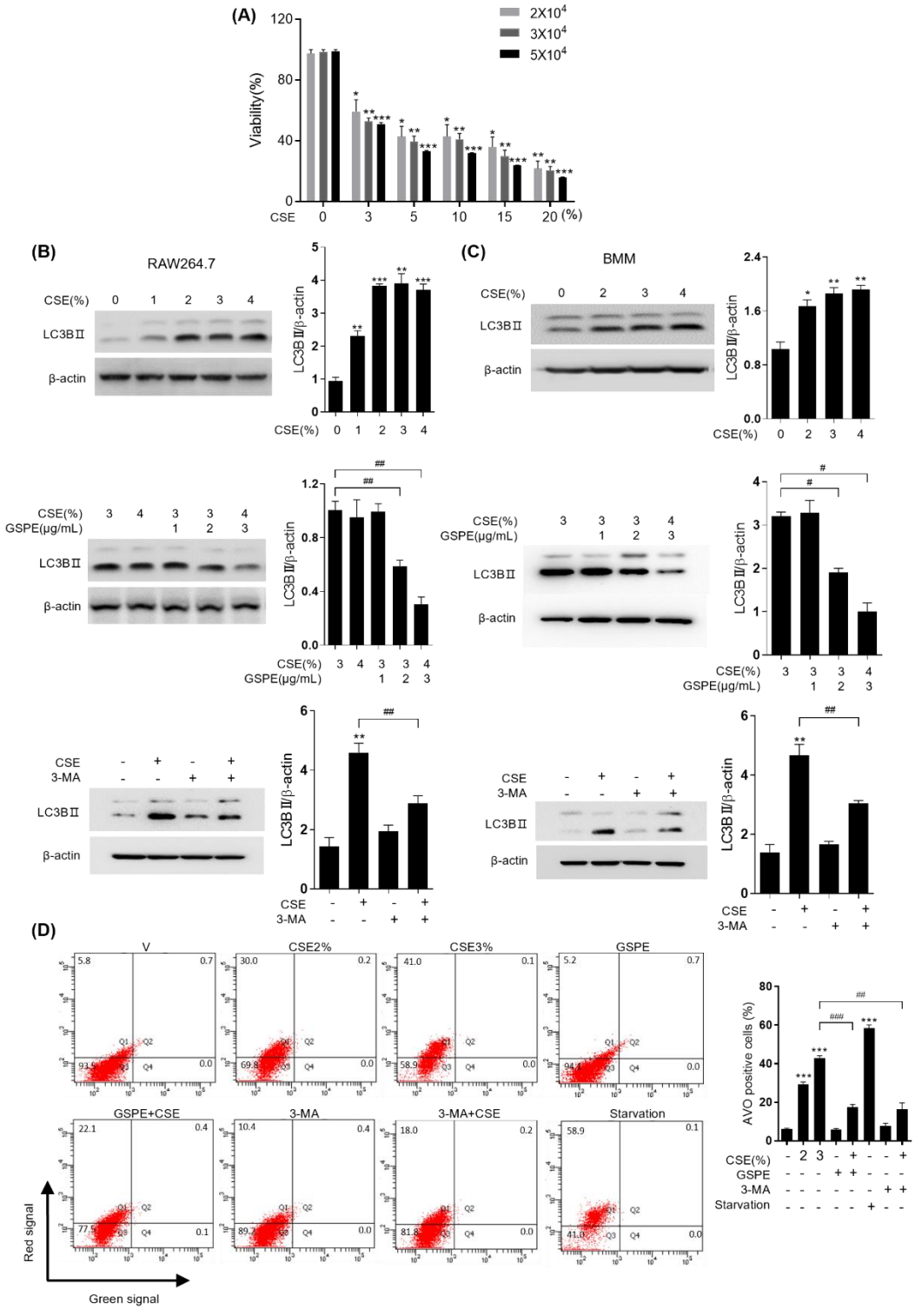

Fig. 2. (continued)

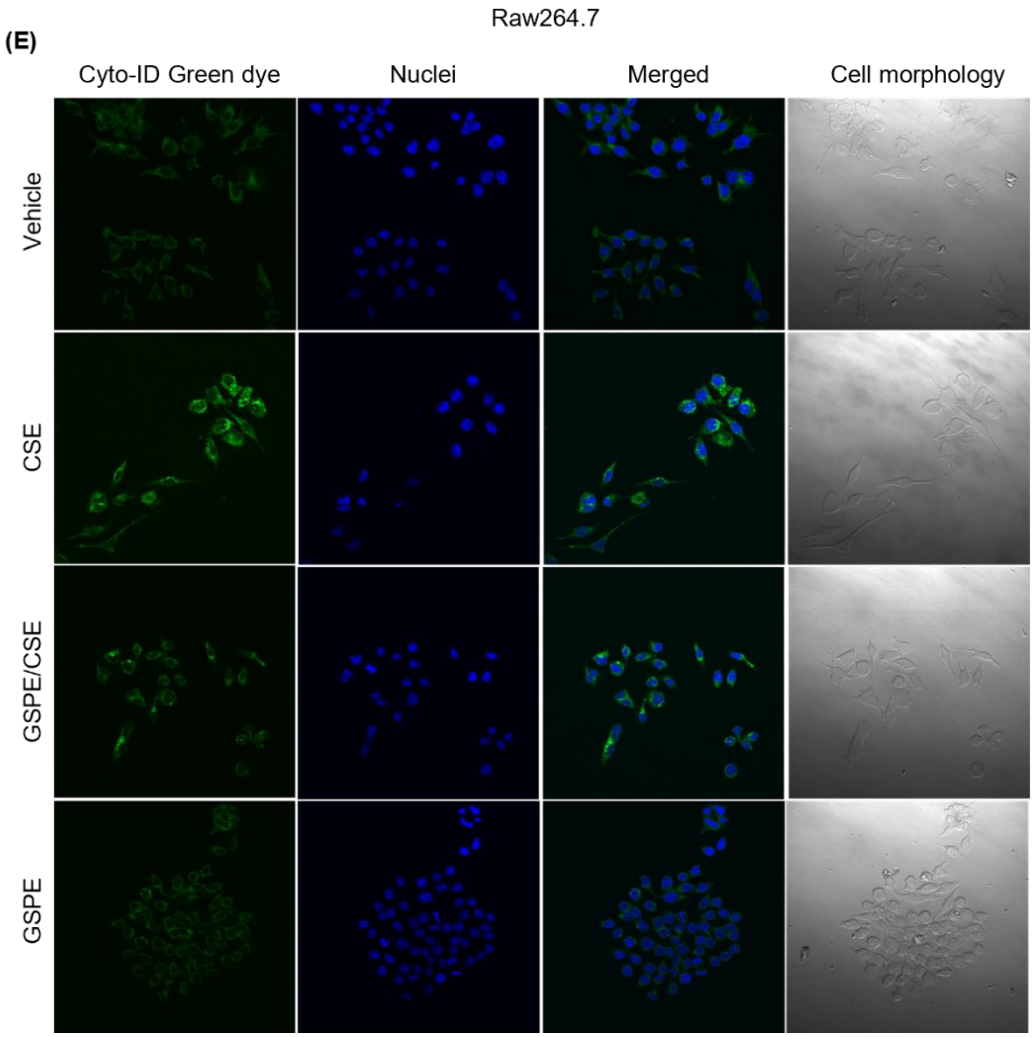

Fig. 2. (continued)

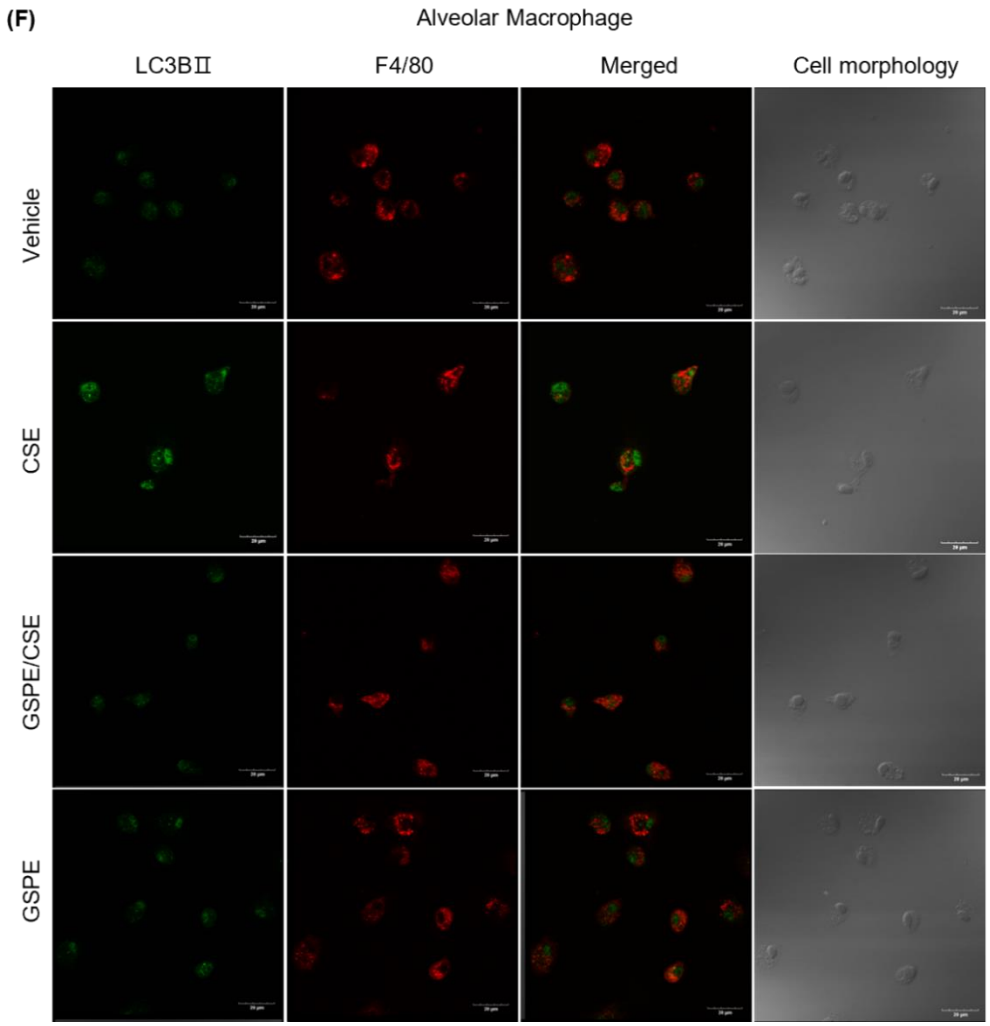

Fig. 2. GSPE attenuates CSE-induced autophagy.

(A) RAW 264.7 cells were treated with CSE at the indicated concentrations (0%, 3%, 5%, 10%, 15%, and 20%) for 24 h. Cell viability was measured using the MTS assay. (B) RAW 264.7 cells and (C) BMMs were subjected to western blot to determine LC3BII expression, which was normalized to that of β-actin. (D) RAW 264.7 cells were stained with AO (1 μg/mL) for 20 min to assess AVO formation and analyzed using flow cytometry. (E) RAW 264.7 cells were stained with Cyto-ID Green dye and Hoechst 33342 for confocal analysis. (F) AMs were immune stained with an APC rat and anti-mouse F4/80 and anti-LC3 antibodies and subsequently detected with Alexa Flour 488 conjugated secondary antibody using a confocal system. Scale bars, 20 μm. Data are representative of three independent experiments. *$p < 0.05$, **$p < 0.01$, ***$p < 0.001$ compared with untreated cells. #$p < 0.05$, ##$p < 0.01$, ###$p < 0.001$ compared with CSE-treated cells.

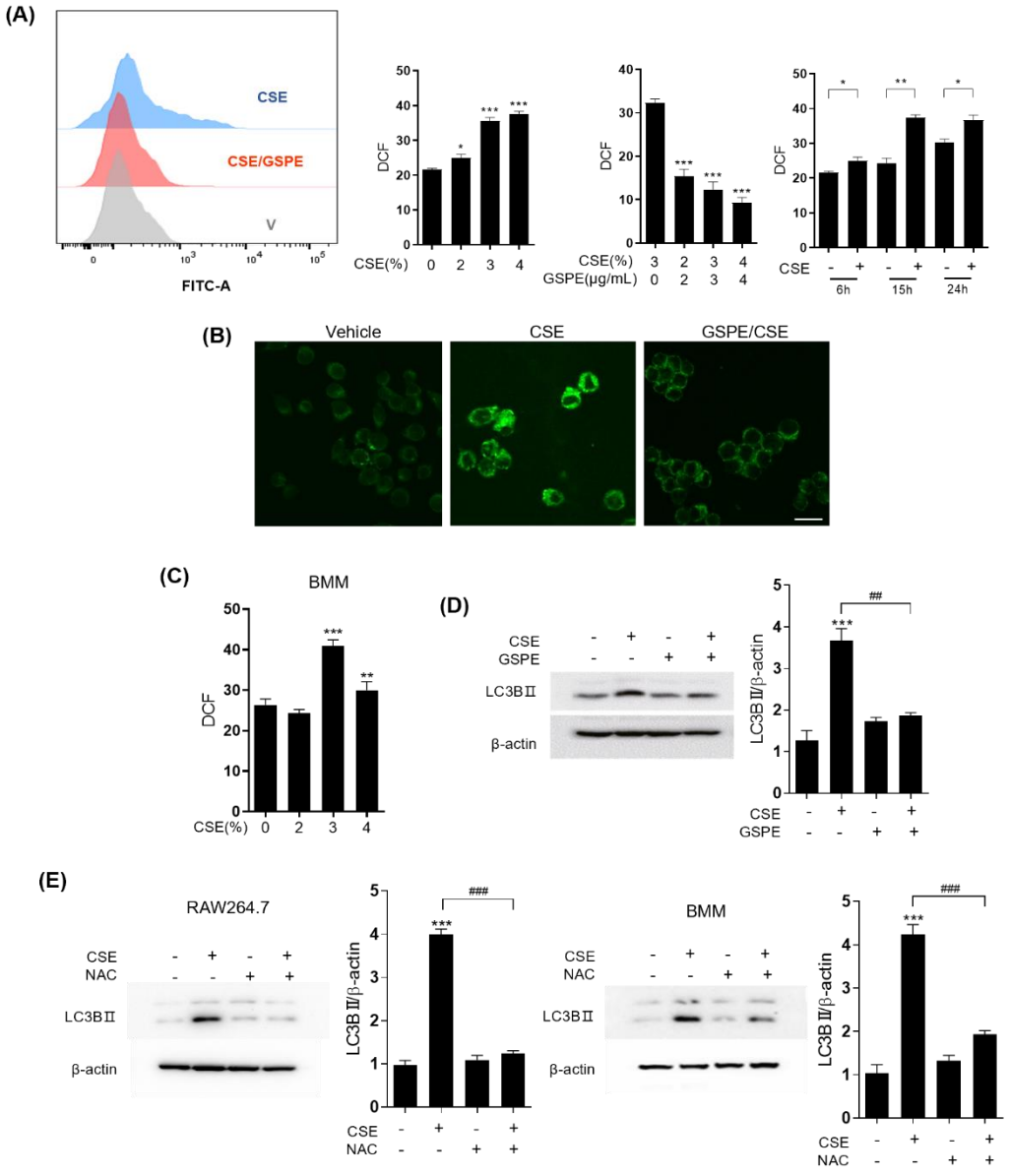

Fig. 3. GSPE inhibits CSE-induced oxidative stress, leading to reduced autophagy.

(A, B) RAW 264.7 cells and (C) BMMs were treated with GSPE (3 μg/mL) for 4 h and then incubated with 3% CSE for 15 h. Intracellular ROS were stained with DCF-DA and analyzed using flow cytometry and confocal microscopy. Scale bars, 20 μm. (D, E) RAW 264.7 cells and BMMs were treated with GSPE (3 μg/mL) or NAC (5 mM) for 4 h before the addition of 3% CSE for 24 h. LC3BII expression was detected by western blot analysis and normalized to that of ß-actin. Data are representative of three independent experiments. *$p < 0.05$, **$p < 0.01$, ***$p < 0.001$ in comparison with nontreated cells. ##$p < 0.01$, ###$p < 0.001$ in comparison with CSE-treated cells.

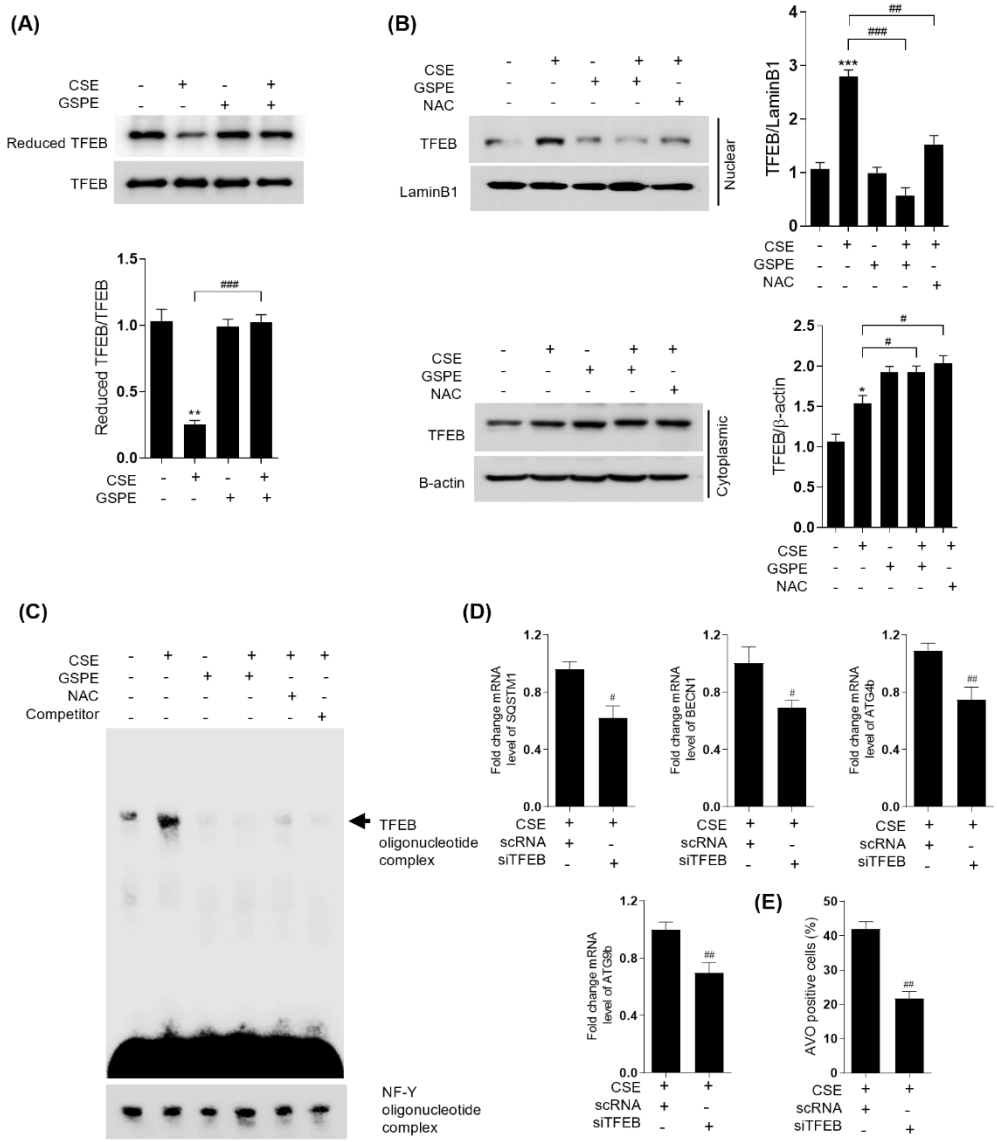

Fig. 4. GSPE reduces CSE-induced TFEB oxidation, resulting in decreased TFEB nuclear translocation.

(A) Raw 264.7 cell lysates were labeled with BIAM, TFEB was immunoprecipitated (IP) from each sample, and HRP-streptavidin immunoblotting was performed to evaluate the reduced form of TFEB. (B) Whole-cell lysates were separated into cytoplasmic and nuclear fractions, followed by western blot analysis with anti-TFEB antibodies. Cytoplasmic and nuclear extracts were normalized using antibodies for β-actin and Lamin B1, respectively. (C) RAW 264.7 cells (8×10^5 cells) were incubated with vehicle (V) (lane 1), CSE (lane 2), GSPE (lane 3), CSE+GSPE (lane 4), or CSE+NAC (lane 5). A 100-fold excess of unlabeled probes

(lane 6) was used as a negative control. The extracts were assayed for TFEB activity by EMSA. NF–Y probe was used as a loading control. (D) The cells were transfected with scRNA or siTFEB and incubated further with 3% CSE. RNA was isolated and analyzed by qPCR. (E) Cells were transfected with scRNA or siTFEB, incubated with 3% CSE for 24 h, and then stained with AO (1 μg/mL) for 20 min before analysis using flow cytometry. Data are representative of three independent experiments. *$p < 0.05$, **$p < 0.01$, ***$p < 0.001$ compared with nontreated cells. #$p < 0.05$, ##$p < 0.01$, ###$p < 0.001$ compared with CSE-treated cells.

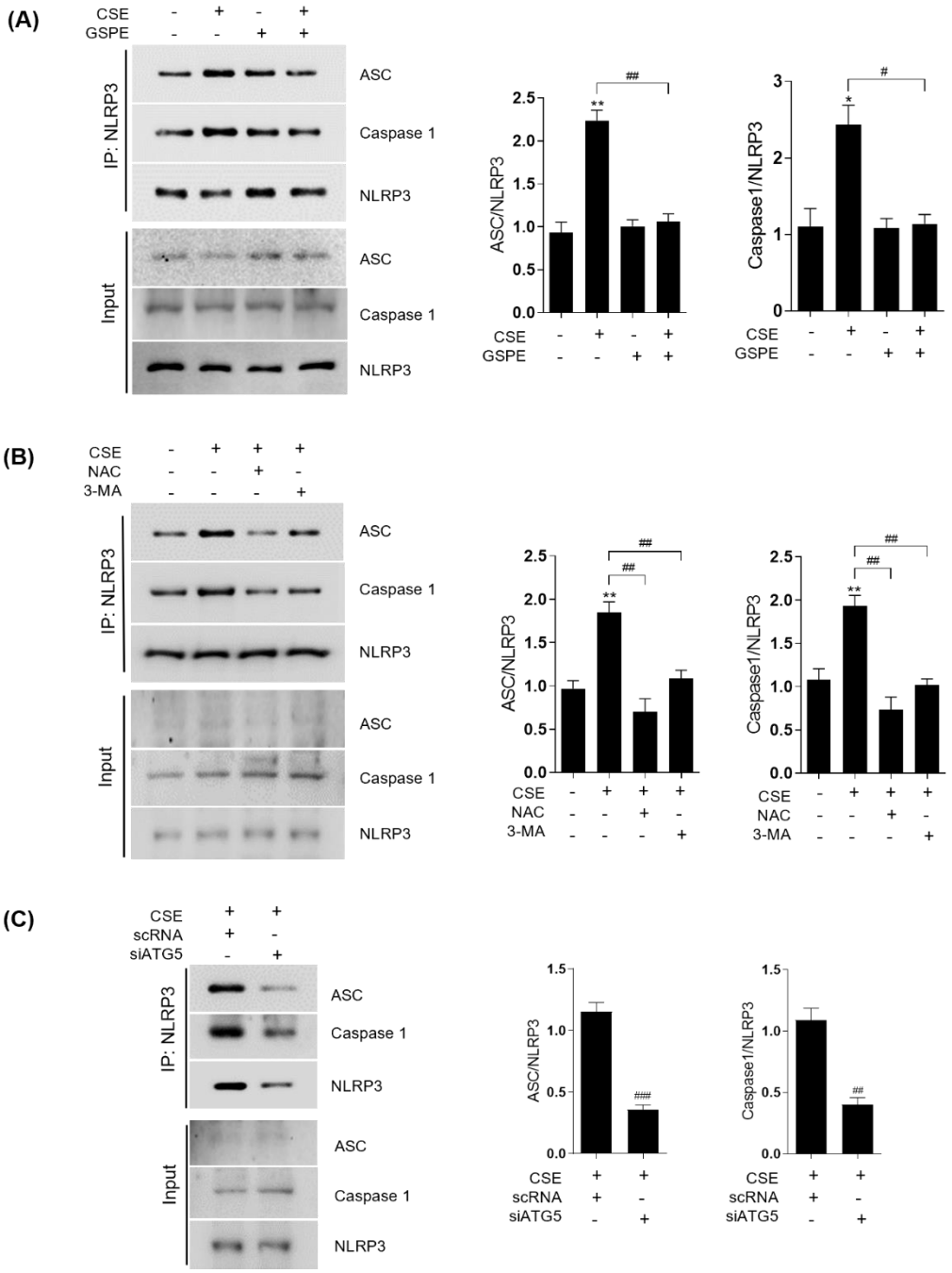

Fig. 5. GSPE attenuates autophagy-induced lung inflammation by inhibiting the NLRP3 inflammasome.

(A) RAW 264.7 cells were treated with GSPE (3 μg/mL) for 4 h and then incubated with 3% CSE for 24 h. (B) RAW 264.7 cells were treated with GSPE (3 μg/mL), 3-MA (100 nM), or NAC (5 mM) for 4 h and then incubated with 3% CSE for 24 h. (C) The cells were transfected with scRNA or siATG5 and incubated further with 3% CSE for 24 h. After whole-cell lysates

were prepared from cultured cells, activation of NLRP3 inflammasome was detected using IP with anti-NLRP3 antibody followed by immunoblotting (IB) for ASC, cleaved caspase-1, and NLRP3 antibodies. Data are representative of three independent experiments. *$p < 0.05$, **$p < 0.01$ compared with nontreated cells. #$p < 0.05$, ##$p < 0.01$, ###$p < 0.001$ compared with CSE-treated cells.

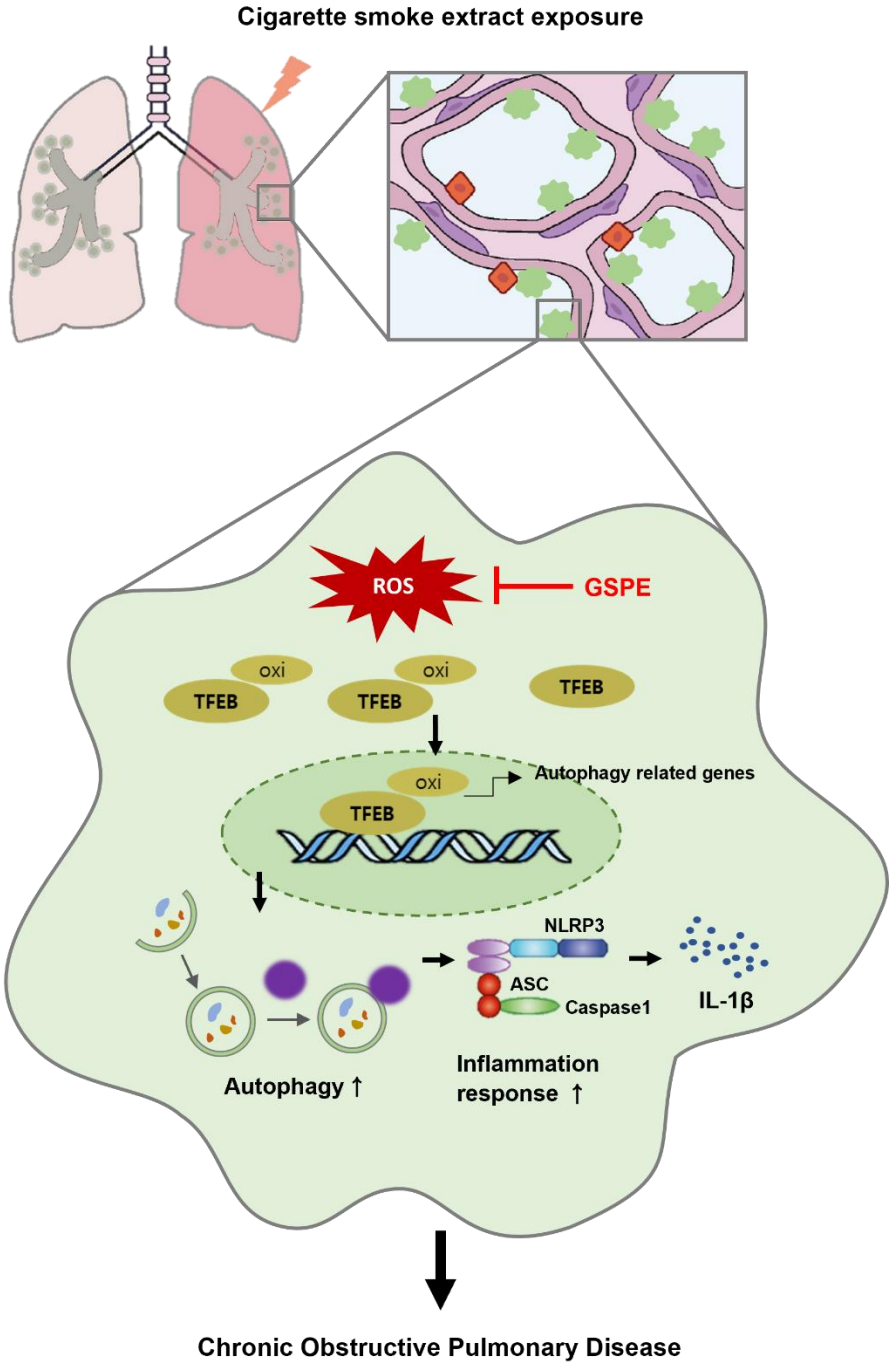

Fig. 6. Schematic diagram of proposed pathways.

GSPE ameliorates lung inflammation and emphysema progression by regulating the autophagy-induced NLRP3 inflammasome through the ROS/TFEB signaling pathway in a COPD mouse model.

Discussion

COPD is a progressive, irreversible inflammatory disease of the lungs that involves small airway inflammation and destruction of lung parenchyma, i.e., emphysema, which leads to airflow limitation [1, 2]. Cigarette smoking is a major risk factor for COPD, leading to significantly elevated ROS generation. CS-induced oxidative stress is an important mechanism underlying COPD pathogenesis, resulting in chronic inflammation of the airways and recruitment of inflammatory cells, primarily AMs and neutrophils. Numerous studies have shown the relationship between oxidative stress and autophagy in COPD [53, 54]. CS exposure is the most common method to build a COPD animal model. However, new modeling methods are being explored constantly because of the long modeling time and instability [55, 56]. CS and CSE induce autophagy, which plays an essential role in the pathogenesis of lung diseases such as COPD [11, 19, 44-46]. Considering that autophagy can be induced with CSE-induced oxidative stress and contributes to lung inflammation and emphysema, we hypothesized that the antioxidant GSPE can inhibit CSE-induced oxidative stress and autophagy, reducing inflammation and emphysema severity. To evaluate the role of GSPE in COPD pathogenesis, we first established a CSE-induced COPD mouse model by intraperitoneally injecting CSE as previously described [36, 57]. CS exposure and CSE intraperitoneal injection can induce emphysema, exhibiting similar effectiveness in constructing the model [36, 57-60]. Intraperitoneal injection of CSE in rats induces emphysematous lung destruction [57, 59, 60], a method that has also been successfully replicated in mice [36, 58]. Finally, CSE injection is not only convenient but also has advantages, such as consistency, stability, and a short modeling time. For these reasons, we selected intraperitoneal CSE injection as a method to establish a COPD mouse model. Our pathologic findings showed the inhibitory effect of GSPE on CSE-induced COPD in mice. GSPE also markedly reduced airspace enlargement, destruction of alveolar walls, release of proinflammatory cytokines, and immune cell infiltration induced by CSE. These results showed that GSPE exerted protective effects on the CSE-induced COPD mouse model by alleviating pathological changes.

Autophagy is a conserved cellular survival mechanism to maintain cellular homeostasis. It plays an important role in overcoming exogenous stress, but prolonged and excessive autophagy can cause irreversible lung injury. Autophagy activation is induced by CS and is closely associated with COPD pathogenesis [11, 12]. However, the role of autophagy in COPD

pathogenesis remains controversial because of its protective and injurious aspects. Thus, the role of autophagy in human diseases is complex. Several studies have reported that autophagy impairment accelerates COPD progression, suggesting that it plays a protective role in CSE-induced COPD pathogenesis [24, 61, 62]. Furthermore, SIRT6 overexpression promotes autophagy, attenuating the senescence of CSE-induced human bronchial tracheal epithelial cells [63]. By contrast, some studies have reported that activation of autophagy aggravates pathological processes, negatively affecting COPD prognosis [26, 53, 64]. Wang et al. found that CSE-induced autophagy activation exacerbates lung damage in COPD [64]. Moreover, Gouzi et al. showed that autophagy inhibition by 3-MA nearly restores the diameter of COPD myotubes to normal [53]. Cigarette smoking promotes the autophagy of lung macrophages, suggesting that excessive autophagy can contribute to lung macrophage dysfunction [65-67]. These studies demonstrated that dysfunction of lung macrophages inhibits phagocytosis and bacterial clearance and enhances the release of inflammatory mediators and proteases [2-4, 26], eventually causing airway inflammation and alveolar destruction. Although further studies are required to elucidate the role of autophagy in COPD, the present data clearly demonstrated that CSE induced significant autophagic flux in cells in comparison with the vehicle. By contrast, GSPE considerably inhibited CSE-induced autophagy in RAW 264.7 cells, BMMs, and AMs. CSE triggered excessive autophagy in macrophages, which could lead to uncontrolled inflammation, whereas GSPE recovered the excessive CSE-induced inflammation by suppressing autophagy.

Recent studies have reported that ROS produced from the mitochondria and NADPH oxidases are vital for autophagy activation [45] and that ROS function as upstream signals in autophagy [68]. Consistent with these findings, the present data showed that CSE markedly increased intracellular ROS levels in macrophages, whereas GSPE treatment significantly decreased the CSE-induced ROS levels. These results indicated that GSPE exhibited antioxidant effects on CSE-induced oxidative stress in macrophages. In addition, GSPE significantly reduced the CSE-induced increase in LC3BII accumulation. Similarly, the ROS scavenger NAC also exerted the same effect. These results suggested that ROS removal by GSPE or NAC significantly diminished the enhancing effect of CSE on autophagy activation, indicating that ROS could be responsible for CSE-induced autophagy in macrophages.

We also determined which molecule was the target for ROS to affect autophagy. Recent studies have indicated that ROS directly oxidize TFEB, which enhances nuclear localization

in oxysterol-induced osteoclasts [69]. TFEB is a key transcription factor regulating autophagy at the transcriptional level and can bind to the promoters of autophagy genes to induce autophagosome formation and autophagosome-lysosome fusion. Our results demonstrated that CSE can increase the oxidized TFEB and nuclear localization of TFEB. By contrast, GSPE could reduce the oxidized TFEB, which subsequently attenuated the CSE-induced increase in TFEB nuclear translocation. The removal of ROS by NAC also clearly abolished the enhancing effect of CSE on TFEB nuclear translocation. These data demonstrated that the CSE-enhanced autophagy activation was mainly mediated by increasing TFEB nuclear translocation through the CSE-induced ROS level in macrophages. However, the antioxidant GSPE ameliorated CSE-induced oxidative stress and TFEB nuclear translocation, leading to autophagy downregulation.

Autophagy ensures balance between innate immunity and inflammation by regulating the release of proinflammatory cytokines [18]. Zhang et al. reported that activation of autophagy in macrophages induces mechanical ventilation-induced lung inflammation through NLRP3 inflammasome signaling [20]. Moreover, autophagy deficiency in macrophages decreases lung and bronchoalveolar immune cell infiltration and cytokine levels in the air space during lipopolysaccharide-induced lung inflammation [21]. However, the exact role of autophagy in the pulmonary macrophages in CSE-induced COPD pathogenesis remains unclear. The NLRP3 inflammasome, primarily expressed in monocytes and macrophages, is a cytosolic multi-protein complex that is a part of the innate immune response. However, overactivation of the NLRP3 inflammasome can lead to various inflammatory diseases, including COPD. In addition, NLRP3 expression is increased by exposure to CS in mouse lung tissue [70-72]. Cao et al. demonstrated that activation of the NLRP3 inflammasome may be associated with CS-induced ROS production [71]. Our data demonstrated that the levels of NLRP3, ASC, and caspase-1 proteins were clearly increased in macrophages exposed to CSE. However, GSPE abolished the CSE-induced increase in the expression of these NLRP3 inflammasome assembly markers. These results indicated that GSPE can mitigate the CSE-induced activation of the NLRP3 inflammasome.

Previous studies have implicated inflammasome-dependent cytokines in COPD pathogenesis. For instance, increasing amounts of NLRP3 and IL-1β are expressed in COPD lungs [73, 74], and CS-exposed NLRP3 knockout mice show reduced production of caspase-1, IL-1β, and IL-18 [75]. IL-1β is a major proinflammatory cytokine that enhances the

production of additional cytokines, such as IL-6. CS triggers the release of IL-1β and other master cytokines, such as TNF-α, IL-6, and IL-8, resulting in macrophage activation in COPD [76]. Consistent with the CSE-induced activation of the NLRP3 inflammasome, our results showed that IL-1β levels significantly increased in the BALF after CSE administration. This result indicated that NLRP3 inflammasome activation during CSE administration contributed to IL-1β release and that CSE can activate the NLRP3/ASC/caspase-1 inflammasome in macrophages. However, the CSE-induced IL-1β production was clearly decreased by GSPE, suggesting that GSPE can ameliorate CSE-mediated inflammasome activation and the subsequent inflammation.

Conclusions

This study demonstrated that CSE-induced ROS production elevated autophagy by enhancing the nuclear translocation of TFEB through oxidized TFEB in macrophages. The excessive autophagy in macrophages enhanced NLRP3 inflammasome activation, contributing to lung inflammation and emphysema progression in a mouse model of COPD. However, GSPE decreased TFEB-oxidizing ROS levels, which reduced TFEB nuclear translocation and autophagy in CSE-treated macrophages and ameliorated the CSE-induced lung inflammation and emphysema in mice. These results demonstrate that GSPE exerted protective effects against inflammation and emphysema in a COPD mouse model by regulating the autophagy-induced NLRP3 inflammasome through the ROS/TFEB signaling pathway.

The work presented here has been published before [77].

References

1. Rabe KF, Hurd S, Anzueto A, Barnes PJ, Buist SA, Calverley P, et al. Global strategy for the diagnosis, management, and prevention of chronic obstructive pulmonary disease: GOLD executive summary. Am J Respir Crit Care Med. 2007;176(6):532-55.
2. Hogg JC, Timens W. The pathology of chronic obstructive pulmonary disease. Annu Rev Pathol. 2009;4:435-59.
3. Rahman I, MacNee W. Role of oxidants/antioxidants in smoking-induced lung diseases. Free Radic Biol Med. 1996;21(5):669-81.
4. Rahman I, Biswas SK, Kode A. Oxidant and antioxidant balance in the airways and airway diseases. Eur J Pharmacol. 2006;533(1-3):222-39.
5. Tuder RM, Yun JH. It takes two to tango: cigarette smoke partners with viruses to promote emphysema. J Clin Invest. 2008;118(8):2689-93.
6. van der Toorn M, Smit-de Vries MP, Slebos DJ, de Bruin HG, Abello N, van Oosterhout AJ, et al. Cigarette smoke irreversibly modifies glutathione in airway epithelial cells. Am J Physiol Lung Cell Mol Physiol. 2007;293(5):L1156-62.
7. van der Toorn M, Rezayat D, Kauffman HF, Bakker SJ, Gans RO, Koëter GH, et al. Lipid-soluble components in cigarette smoke induce mitochondrial production of reactive oxygen species in lung epithelial cells. Am J Physiol Lung Cell Mol Physiol. 2009;297(1):L109-14.
8. Doll R. Risk from tobacco and potentials for health gain. Int J Tuberc Lung Dis. 1999;3(2):90-9.
9. Hodge S, Matthews G, Mukaro V, Ahern J, Shivam A, Hodge G, et al. Cigarette smoke-induced changes to alveolar macrophage phenotype and function are improved by treatment with procysteine. Am J Respir Cell Mol Biol. 2011;44(5):673-81.
10. Franke-Ullmann G, Pförtner C, Walter P, Steinmüller C, Lohmann-Matthes ML, Kobzik L. Characterization of murine lung interstitial macrophages in comparison with alveolar macrophages in vitro. J Immunol. 1996;157(7):3097-104.
11. Hwang JW, Chung S, Sundar IK, Yao H, Arunachalam G, McBurney MW, et al. Cigarette smoke-induced autophagy is regulated by SIRT1-PARP-1-dependent mechanism: implication in pathogenesis of COPD. Arch Biochem Biophys. 2010;500(2):203-9.

12. Li L, Zhang M, Zhang L, Cheng Y, Tu X, Lu Z. Klotho regulates cigarette smoke-induced autophagy: Implication in pathogenesis of COPD. Lung. 2017;195(3):295-301.
13. Kapellos TS, Bassler K, Aschenbrenner AC, Fujii W, Schultze JL. Dysregulated functions of lung macrophage populations in COPD. J Immunol Res. 2018;2018:2349045.
14. Yamasaki K, Eeden SFV. Lung macrophage phenotypes and functional responses: Role in the pathogenesis of COPD. Int J Mol Sci. 2018;19(2).
15. Codogno P, Meijer AJ. Autophagy and signaling: their role in cell survival and cell death. Cell Death Differ. 2005;12 Suppl 2:1509-18.
16. Lo S, Yuan SS, Hsu C, Cheng YJ, Chang YF, Hsueh HW, et al. Lc3 over-expression improves survival and attenuates lung injury through increasing autophagosomal clearance in septic mice. Ann Surg. 2013;257(2):352-63.
17. Chen ZH, Lam HC, Jin Y, Kim HP, Cao J, Lee SJ, et al. Autophagy protein microtubule-associated protein 1 light chain-3B (LC3B) activates extrinsic apoptosis during cigarette smoke-induced emphysema. Proc Natl Acad Sci U S A. 2010;107(44):18880-5.
18. Levine B, Mizushima N, Virgin HW. Autophagy in immunity and inflammation. Nature. 2011;469(7330):323-35.
19. Chen ZH, Kim HP, Sciurba FC, Lee SJ, Feghali-Bostwick C, Stolz DB, et al. Egr-1 regulates autophagy in cigarette smoke-induced chronic obstructive pulmonary disease. PLoS One. 2008;3(10):e3316.
20. Zhang Y, Liu G, Dull RO, Schwartz DE, Hu G. Autophagy in pulmonary macrophages mediates lung inflammatory injury via NLRP3 inflammasome activation during mechanical ventilation. Am J Physiol Lung Cell Mol Physiol. 2014;307(2):L173-85.
21. Guo L, Stripay JL, Zhang X, Collage RD, Hulver M, Carchman EH, et al. CaMKIα regulates AMP kinase-dependent, TORC-1-independent autophagy during lipopolysaccharide-induced acute lung neutrophilic inflammation. J Immunol. 2013;190(7):3620-8.
22. Lamkanfi M, Dixit VM. Inflammasomes: guardians of cytosolic sanctity. Immunol Rev. 2009;227(1):95-105.
23. Tschopp J, Schroder K. NLRP3 inflammasome activation: The convergence of

multiple signalling pathways on ROS production? Nat Rev Immunol. 2010;10(3):210-5.

24. Vij N, Chandramani-Shivalingappa P, Van Westphal C, Hole R, Bodas M. Cigarette smoke-induced autophagy impairment accelerates lung aging, COPD-emphysema exacerbations and pathogenesis. Am J Physiol Cell Physiol. 2018;314(1):C73-c87.

25. Cao L, Xu J, Lin Y, Zhao X, Liu X, Chi Z. Autophagy is upregulated in rats with status epilepticus and partly inhibited by Vitamin E. Biochem Biophys Res Commun. 2009;379(4):949-53.

26. Lam HC, Cloonan SM, Bhashyam AR, Haspel JA, Singh A, Sathirapongsasuti JF, et al. Histone deacetylase 6-mediated selective autophagy regulates COPD-associated cilia dysfunction. J Clin Invest. 2013;123(12):5212-30.

27. Mizumura K, Cloonan SM, Nakahira K, Bhashyam AR, Cervo M, Kitada T, et al. Mitophagy-dependent necroptosis contributes to the pathogenesis of COPD. J Clin Invest. 2014;124(9):3987-4003.

28. Hao R, Li Q, Zhao J, Li H, Wang W, Gao J. Effects of grape seed procyanidins on growth performance, immune function and antioxidant capacity in weaned piglets. Livest Sci. 2015;178:237-42.

29. Feng LL, Liu BX, Zhong JY, Sun LB, Yu HS. Effect of grape procyanidins on tumor angiogenesis in liver cancer xenograft models. Asian Pac J Cancer Prev. 2014;15(2):737-41.

30. Akiyama H, Sakushima J, Taniuchi S, Kanda T, Yanagida A, Kojima T, et al. Antiallergic effect of apple polyphenols on the allergic model mouse. Biol Pharm Bull. 2000;23(11):1370-3.

31. Nishizuka T, Fujita Y, Sato Y, Nakano A, Kakino A, Ohshima S, et al. Procyanidins are potent inhibitors of LOX-1: a new player in the French Paradox. Proc Jpn Acad Ser B Phys Biol Sci. 2011;87(3):104-13.

32. Belcaro G, Ledda A, Hu S, Cesarone MR, Feragalli B, Dugall M. Grape seed procyanidins in pre- and mild hypertension: a registry study. Evid Based Complement Alternat Med. 2013;2013:313142.

33. Kimmel EM, Jerome M, Holderness J, Snyder D, Kemoli S, Jutila MA, et al. Oligomeric procyanidins stimulate innate antiviral immunity in dengue virus infected human PBMCs. Antiviral Res. 2011;90(1):80-6.

34. Ray SD, Patel D, Wong V, Bagchi D. In vivo protection of dna damage associated apoptotic and necrotic cell deaths during acetaminophen-induced nephrotoxicity, amiodarone-induced lung toxicity and doxorubicin-induced cardiotoxicity by a novel IH636 grape seed proanthocyanidin extract. Res Commun Mol Pathol Pharmacol. 2000;107(1-2):137-66.
35. Sul OJ, Kim JH, Lee T, Seo KW, Cha HJ, Kwon B, et al. GSPE protects against bleomycin-induced pulmonary fibrosis in mice via ameliorating epithelial apoptosis through inhibition of oxidative stress. Oxid Med Cell Longev. 2022;2022:8200189.
36. Zhang Y, Cao J, Chen Y, Chen P, Peng H, Cai S, et al. Intraperitoneal injection of cigarette smoke extract induced emphysema, and injury of cardiac and skeletal muscles in BALB/C mice. Exp Lung Res. 2013;39(1):18-31.
37. Alzoubi A, Ghazwi R, Alzoubi K, Alqudah M, Kheirallah K, Khabour O, et al. Vascular endothelial growth factor receptor inhibition enhances chronic obstructive pulmonary disease picture in mice exposed to waterpipe smoke. Folia Morphol (Warsz). 2018;77(3):447-55.
38. Sul OJ, Kim JE, Ke K, Suh JH, Choi HS. Atherogenic diet-induced bone loss is primarily due to increased osteoclastogenesis in mice. J Nutr Biochem. 2020;79:108337.
39. Bil J, Winiarska M, Nowis D, Bojarczuk K, Dabrowska-Iwanicka A, Basak GW, et al. Bortezomib modulates surface CD20 in B-cell malignancies and affects rituximab-mediated complement-dependent cytotoxicity. Blood. 2010;115(18):3745-55.
40. Bagchi D, Garg A, Krohn RL, Bagchi M, Tran MX, Stohs SJ. Oxygen free radical scavenging abilities of vitamins C and E, and a grape seed proanthocyanidin extract in vitro. Res Commun Mol Pathol Pharmacol. 1997;95(2):179-89.
41. Ito S, Ingenito EP, Arold SP, Parameswaran H, Tgavalekos NT, Lutchen KR, et al. Tissue heterogeneity in the mouse lung: effects of elastase treatment. J Appl Physiol (1985). 2004;97(1):204-12.
42. Finicelli M, Digilio FA, Galderisi U, Peluso G. The emerging role of macrophages in chronic obstructive pulmonary disease: The potential impact of oxidative stress and extracellular vesicle on macrophage polarization and function. Antioxidants (Basel). 2022;11(3).
43. Barnes PJ. Alveolar macrophages as orchestrators of COPD. Copd. 2004;1(1):59-70.

44. Zhu X, Zhan Y, Gu Y, Huang Q, Wang T, Deng Z, et al. Cigarette smoke promotes interleukin-8 production in alveolar macrophages through the reactive oxygen species/stromal interaction molecule 1/Ca(2+) axis. Front Physiol. 2021;12:733650.
45. Scherz-Shouval R, Shvets E, Fass E, Shorer H, Gil L, Elazar Z. Reactive oxygen species are essential for autophagy and specifically regulate the activity of Atg4. Embo j. 2007;26(7):1749-60.
46. Chen Y, McMillan-Ward E, Kong J, Israels SJ, Gibson SB. Oxidative stress induces autophagic cell death independent of apoptosis in transformed and cancer cells. Cell Death Differ. 2008;15(1):171-82.
47. Kim S, Song G, Lee T, Kim M, Kim J, Kwon H, et al. PARsylated transcription factor EB (TFEB) regulates the expression of a subset of Wnt target genes by forming a complex with β-catenin-TCF/LEF1. Cell Death Differ. 2021;28(9):2555-70.
48. Settembre C, Di Malta C, Polito VA, Garcia Arencibia M, Vetrini F, Erdin S, et al. TFEB links autophagy to lysosomal biogenesis. Science. 2011;332(6036):1429-33.
49. Di Malta C, Cinque L, Settembre C. Transcriptional regulation of autophagy: Mechanisms and diseases. Front Cell Dev Biol. 2019;7:114.
50. Rumora L, Hlapčić I, Hulina-Tomašković A, Somborac-Bačura A, Bosnar M, Rajković MG. Pathogen-associated molecular patterns and extracellular Hsp70 interplay in NLRP3 inflammasome activation in monocytic and bronchial epithelial cellular models of COPD exacerbations. Apmis. 2021;129(2):80-90.
51. Ji S, Bai Q, Wu X, Zhang DW, Wang S, Shen JL, et al. Unique synergistic antiviral effects of Shufeng Jiedu Capsule and oseltamivir in influenza A viral-induced acute exacerbation of chronic obstructive pulmonary disease. Biomed Pharmacother. 2020;121:109652.
52. Yang Y, Wang H, Kouadir M, Song H, Shi F. Recent advances in the mechanisms of NLRP3 inflammasome activation and its inhibitors. Cell Death Dis. 2019;10(2):128.
53. Gouzi F, Blaquière M, Catteau M, Bughin F, Maury J, Passerieux E, et al. Oxidative stress regulates autophagy in cultured muscle cells of patients with chronic obstructive pulmonary disease. J Cell Physiol. 2018;233(12):9629-39.
54. Wang Y, Chen J, Chen W, Liu L, Dong M, Ji J, et al. LINC00987 ameliorates COPD by regulating LPS-induced cell apoptosis, oxidative stress, inflammation and autophagy through Let-7b-5p/SIRT1 axis. Int J Chron Obstruct Pulmon Dis.

2020;15:3213-25.

55. Ghorani V, Boskabady MH, Khazdair MR, Kianmeher M. Experimental animal models for COPD: a methodological review. Tob Induc Dis. 2017;15:25.

56. Wright JL, Churg A. Animal models of cigarette smoke-induced chronic obstructive pulmonary disease. Expert Rev Respir Med. 2010;4(6):723-34.

57. Chen Y, Hanaoka M, Chen P, Droma Y, Voelkel NF, Kubo K. Protective effect of beraprost sodium, a stable prostacyclin analog, in the development of cigarette smoke extract-induced emphysema. Am J Physiol Lung Cell Mol Physiol. 2009;296(4):L648-56.

58. He ZH, Chen P, Chen Y, He SD, Ye JR, Zhang HL, et al. Comparison between cigarette smoke-induced emphysema and cigarette smoke extract-induced emphysema. Tob Induc Dis. 2015;13(1):6.

59. Liu Y, Li A, Feng X, Jiang X, Sun X, Huang W, et al. l-Menthol alleviates cigarette smoke extract induced lung injury in rats by inhibiting oxidative stress and inflammation via nuclear factor kappa B, p38 MAPK and Nrf2 signalling pathways. RSC Adv. 2018;8(17):9353-63.

60. Devi K, Moharana B. Cigarette smoke extract triggers neoplastic change in lungs and impairs locomotor activity through wnt3a-β-catenin signaling in aged COPD rodent model. Exp Lung Res. 2020;46(8):283-96.

61. Fujii S, Hara H, Araya J, Takasaka N, Kojima J, Ito S, et al. Insufficient autophagy promotes bronchial epithelial cell senescence in chronic obstructive pulmonary disease. Oncoimmunology. 2012;1(5):630-41.

62. Kuwano K, Araya J, Hara H, Minagawa S, Takasaka N, Ito S, et al. Cellular senescence and autophagy in the pathogenesis of chronic obstructive pulmonary disease (COPD) and idiopathic pulmonary fibrosis (IPF). Respir Investig. 2016;54(6):397-406.

63. Takasaka N, Araya J, Hara H, Ito S, Kobayashi K, Kurita Y, et al. Autophagy induction by SIRT6 through attenuation of insulin-like growth factor signaling is involved in the regulation of human bronchial epithelial cell senescence. J Immunol. 2014;192(3):958-68.

64. Wang Y, Liu J, Zhou JS, Huang HQ, Li ZY, Xu XC, et al. MTOR suppresses cigarette smoke-induced epithelial cell death and airway inflammation in chronic obstructive

pulmonary disease. J Immunol. 2018;200(8):2571-80.

65. Chen P, Cescon M, Bonaldo P. Autophagy-mediated regulation of macrophages and its applications for cancer. Autophagy. 2014;10(2):192-200.

66. Sarkar A, Tindle C, Pranadinata RF, Reed S, Eckmann L, Stappenbeck TS, et al. ELMO1 regulates autophagy induction and bacterial clearance during enteric infection. J Infect Dis. 2017;216(12):1655-66.

67. Bai X, Stitzel JA, Bai A, Zambrano CA, Phillips M, Marrack P, et al. Nicotine impairs macrophage control of Mycobacterium tuberculosis. Am J Respir Cell Mol Biol. 2017;57(3):324-33.

68. Cao Y, Fang Y, Cai J, Li X, Xu F, Yuan N, et al. ROS functions as an upstream trigger for autophagy to drive hematopoietic stem cell differentiation. Hematology. 2016;21(10):613-8.

69. Sul OJ, Li G, Kim JE, Kim ES, Choi HS. 7-ketocholesterol enhances autophagy via the ROS-TFEB signaling pathway in osteoclasts. J Nutr Biochem. 2021;96:108783.

70. Mahalanobish S, Dutta S, Saha S, Sil PC. Melatonin induced suppression of ER stress and mitochondrial dysfunction inhibited NLRP3 inflammasome activation in COPD mice. Food Chem Toxicol. 2020;144:111588.

71. Cao Y, Zhou X, Yin Z, Yu X, Yang Q, Guo Q, et al. The anti-inflammatory effect of BML-111 on COPD may be mediated by regulating NLRP3 inflammasome activation and ROS production. Prostaglandins Other Lipid Mediat. 2018;138:23-30.

72. Yang W, Ni H, Wang H, Gu H. NLRP3 inflammasome is essential for the development of chronic obstructive pulmonary disease. Int J Clin Exp Pathol. 2015;8(10):13209-16.

73. Faner R, Sobradillo P, Noguera A, Gomez C, Cruz T, López-Giraldo A, et al. The inflammasome pathway in stable COPD and acute exacerbations. ERJ Open Res. 2016;2(3).

74. Kim RY, Pinkerton JW, Gibson PG, Cooper MA, Horvat JC, Hansbro PM. Inflammasomes in COPD and neutrophilic asthma. Thorax. 2015;70(12):1199-201.

75. Eltom S, Belvisi MG, Stevenson CS, Maher SA, Dubuis E, Fitzgerald KA, et al. Role of the inflammasome-caspase1/11-IL-1/18 axis in cigarette smoke driven airway inflammation: an insight into the pathogenesis of COPD. PLoS One. 2014;9(11):e112829.

76. Laniado-Laborín R. Smoking and chronic obstructive pulmonary disease (COPD). Parallel epidemics of the 21 century. Int J Environ Res Public Health. 2009;6(1):209-24.

77. Sul OJ, Choi HW, Oh J, Ra SW. GSPE attenuates CSE-induced lung inflammation and emphysema by regulating autophagy via the reactive oxygen species/TFEB signaling pathway. Food Chem Toxicol. 2023;177:113795.

국문 요약

만성 폐쇄성 폐질환(COPD: Chronic Obstructive Pulmonary Disease)은 기류제한, 만성염증, 폐포벽 파괴 및 폐포 공간 확장을 통한 폐기종의 발생을 특징으로 하는 폐질환이다. 유해입자나 가스, 특히 담배연기(CS: Cigarette Smoke)는 이 질환의 위험인자로 알려져 있다. CS 는 염증 및 상피세포에서 활성산소(ROS: reactive oxygen species)의 생성을 증가시킬 수 있으며, 이는 산화 스트레스와 염증으로 이어져 COPD 를 유발할 수 있는 것으로 알려져 있다. 그러나 COPD 의 정확한 발병기전은 아직 완전히 밝혀지지 않고 있다.

이에 본 연구는 포도씨 프로안토시아니딘 추출물(GSPE: that grape seed proanthocyanidin extract)이 항산화제로서 작용하여, 대식세포의 산화 스트레스의 억제를 통해 담배 연기 추출물(CSE: Cigarette Smoke Extract)로 인한 자가포식 활성화와 염증반응을 개선함으로써 폐기종을 완화할 수 있는 가를 알아보고자 하였다.

본 연구에서는 GSPE 의 폐 손상 억제 효과를 확인하기 위해 RAW 264.7 세포, 골수유래 대식세포, 폐포 대식세포, 그리고 CSE 가 유도하는 COPD 마우스 모델에 CSE 와 GSPE 를 처리한 후 나타나는 변화를 관찰하였다. *In vitro* 실험에서, CSE 에 의한 대식세포의 세포독성, ROS, autophagy, 그리고 inflammation 을 측정했으며, *in vivo* 실험에서는 기관지폐포세척액(BALF: bronchoalveolar lavage fluid)을 통한 전염증성 사이토카인 측정과 폐 조직 분리 및 염색을 통한 면역 세포 침윤과 폐 조직 손상도 평가를 진행하였다.

In vivo 실험에서 CSE 의 처리는 폐 손상도와 면역세포의 침윤 그리고 BALF 에서의 전염증성 사이토카인 수준을 증가시켰지만, GSPE 의 전처리는 CSE 에 의한 조직학적 변화와 염증반응을 억제했다. 또한 *in vitro* 실험을 통해 CSE 처리는 ROS 생성을 증가시키고 GSPE 는 이를 감소시킴을 확인했다. 뿐만 아니라 GSPE 는 ROS 의 억제를 통해 CSE 에 의한 transcription factor EB (TFEB) 산화 및 핵으로의 이동을 감소시켜, 자가포식과 관련된 유전자의 발현을 하향 조절했다. CSE 에 의해 유도된 자가포식은 NLRP3 염증복합체를 활성화하여 결국 염증반응을 상향 조절한 반면,

GSPE 는 CSE 에 의한 자가포식과 염증반응을 억제함을 확인했다.

결론적으로 본 연구는 CSE 가 유도하는 COPD 마우스 모델에서 CSE 는 폐포 대식세포에서 산화 스트레스를 증가시키고 TFEB 의 산화와 핵 전위를 유도하여, 자가포식을 활성화하고 결국 염증반응을 활성화함을 입증하였다. 뿐만 아니라 GSPE 가 ROS/TFEB 신호 전달 경로를 통해 자가포식이 유도하는 NLRP3 염증복합체 활성화를 억제함으로써, CSE 로 유발된 COPD 마우스 모델에서 염증과 폐기종 발병을 완화하는데 효과적인 역할을 함을 시사한다.

중심단어 : 만성폐쇄성폐질환, 담배 연기 추출물, 포도씨 프로안토시아니딘 추출물, 염증, 폐기종, 산화 스트레스, 자가포식